Ultrafast Photoinduced Charge Separation in Naphthalene Diimide Based Multichromophoric Systems in Liquid Solutions and in a Lipid Membrane

Natalie Banerji,[†] Alexandre Fürstenberg,[†] Sheshanath Bhosale,[‡] Adam L. Sisson,[‡] Naomi Sakai,[‡] Stefan Matile,[‡] and Eric Vauthey*,[†]

Department of Physical Chemistry, and Department of Organic Chemistry, University of Geneva, 30 Quai Ernest-Ansermet, CH-1211 Geneva 4, Switzerland

Received: February 13, 2008; Revised Manuscript Received: April 19, 2008

The photophysical properties of multichromophoric systems consisting of eight red or blue naphthalene diimides (NDIs) covalently attached to a *p*-octiphenyl scaffold, as well as a blue bichromophoric system with a biphenyl scaffold, have been investigated in detail using femtosecond time-resolved spectroscopy. The blue octachromophoric systems have been recently shown to self-assemble as supramolecular tetramers in lipid bilayer membranes and to enable generation of a transmembrane proton gradient upon photoexcitation (Bhosale, S.; Sisson, A. L.; Talukdar, P.; Fürstenberg, A.; Banerji, N.; Vauthey, E.; Bollot, G.; Mareda, J.; Röger, C.; Würthner, F.; Sakai, N.; Matile, S. *Science* 2006, *313*, 84). A strong reduction of the fluorescence quantum yield was observed when going from the single NDI units to the multichromophoric systems in methanol, the effect being even stronger in a vesicular lipid membrane. Fluorescence up-conversion measurements reveal ultrafast self-quenching in the multichromophoric systems, whereas the formation of the NDI radical anion, evidenced by transient absorption measurements, points to the occurrence of photoinduced charge separation. The location of the positive charge could not be established unambiguously from the transient absorption measurements, but energetic considerations indicate that charge separation should occur between two NDI units in the blue systems, whereas both an NDI unit and the *p*-octiphenyl scaffold could act as electron donor in the red system. The lifetime of the charge-separated state was found to increase from 22 to 45 ps by going from the bi- to the octachromophoric blue systems in methanol, while a 400 ps decay component was observed in the lipid membrane. This lifetime lengthening is explained in terms of charge migration that is most efficient when the octachromophoric systems are assembled as supramolecular tetramers in the lipid membrane. Furthermore, the average charge-separated state lifetime of the red system in methanol is even larger and amounts to 750 ps. This effect cannot be simply explained in terms of Marcus inverted regime as the driving force for charge recombination in the red system is only slightly larger than in the blue one. A better spatial separation of the charges in the red system stemming from the localization of the hole on the *p*-octiphenyl scaffold could additionally contribute to the slowing down of charge recombination.

Introduction

Over the past years, a large number of molecular systems consisting of two or more identical and covalently linked chromophores have been synthesized and investigated. One major motivation was the elaboration of artificial analogues of the light-harvesting complexes of photosynthetic organisms.[1–7] However, multichromophoric molecules have also been developed for other applications such as, for example, molecular wires,[8,9] single photon sources,[10] logic gates,[11] light stabilizers,[12] fluorescent DNA probes,[13,14] or nonlinear optical materials.[15]

The covalent bonding allows the degree of interaction between the chromophoric units to be controlled to some extent. In the strong interaction limit, the chromophores lose their individual character and properties. For example, the electronic absorption and emission spectra as well as the fluorescence quantum yield differ substantially from those of the isolated chromophores as a consequence of the delocalization of excitation over several units. On the other hand, in the weak interaction limit, excitation is localized on a single chromophore, and thus the absorption and emission spectra are essentially the same as those of an individual unit. In this case, however, a modest interaction between the chromophoric moieties is sufficient to enable efficient excitation energy hopping over the whole system, as observed, for example, in the light-harvesting complexes of photosynthetic bacteria[16] and in many artificial analogues.[1–7]

Although excitation energy hopping is a major process in these systems, photoinduced charge separation (CS) between two chemically identical chromophores can also be operative in some cases. For example, the self-quenching of perylene fluorescence has been shown to lead to the formation of both perylene radical cation and anion.[17] Such a symmetry-breaking CS process has also been observed upon excitation of bichromophoric molecules like bianthryl,[18] perylene mono- and diimide dimers,[19,20] and π-stacked perylenediimides.[20,21]

We report here on the investigation of the photophysics of two octachromophoric systems consisting of a *p*-octiphenyl scaffold bearing eight core-substituted naphthalene diimides (NDIs), using femtosecond-resolved fluorescence up-conversion and transient absorption (TA) spectroscopy. The photophysics of N-substituted NDIs has already been investigated in detail.[22–28] These compounds are colorless, their first absorption band being

* Corresponding author. E-mail: eric.vauthey@chiphy.unige.ch.
[†] Department of Physical Chemistry.
[‡] Department of Organic Chemistry.

10.1021/jp801276p CCC: $40.75
Published on Web 07/03/2008

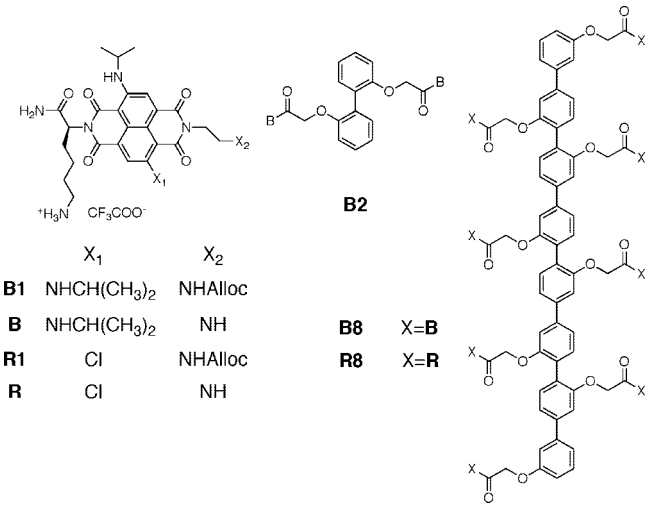

	X_1	X_2
B1	$NHCH(CH_3)_2$	NHAlloc
B	$NHCH(CH_3)_2$	NH
R1	Cl	NHAlloc
R	Cl	NH

Figure 1. Structure of the multichromophoric systems (R and R1 consist in both 2,6- and 3,7-regioisomers, Alloc: allyloxycarbonyl).

located below 400 nm, and very weakly fluorescent because of fast intersystem crossing favored by the strong spin−orbit coupling introduced by the carbonyl groups. N-Substituted NDIs are often used as building blocks in dyads, triads, and donor−bridge−acceptor systems where they act as electron acceptor,[29–33] but their fast intersystem crossing prevents their use as light absorbers. The excited-state properties of these NDIs are essentially independent of the nature of the N-substituents. On the other hand, core substitution has recently been shown to substantially affect the photophysical and electrochemical properties of NDIs.[34,35] Variation of the substituents from amino to alkoxy groups at the 2 and 6 positions on the naphthalene core allows color tuning of the NDIs from blue to yellow.[34] Furthermore, these core-substituted NDIs are strongly emissive, with fluorescence quantum yields on the order of 0.5. These properties are due to an electronic transition of charge-transfer type involving substantial redistribution of the electronic density from the core substituents to the carbonyl groups. Thus, variation of the electron-donating properties of the core substituents enables fine-tuning of the transition energy.

The octachromophoric systems investigated here differ by the core substitution on the NDI moieties, the NDI with two amino substituents being blue and that with one amino substituent and one chlorine atom substituent being red (Figure 1). The blue octachromophoric systems (B8) have recently been shown to self-assemble as tetramers, $B8_4$, in the lipid bilayer membrane of large unilamellar vesicles (LUVs) and to enable generation of a transmembrane proton gradient upon photoexcitation.[36,37] This process was proposed to originate from CS between two NDI moieties, followed by hopping of the charges over the NDI units of $B8_4$, and finally by electron transfer to a secondary acceptor inside the LUV and hole transfer to a secondary donor outside the LUV. This mechanism was supported by TA measurements with B8 in bulk solution, which evidenced the occurrence of photoinduced CS. More detailed investigations of the photophysics of B8 as well as measurements of the excited-state dynamics of $B8_4$ in an LUV membrane are reported here. We will show that both CS and charge recombination (CR) dynamics in $B8_4$ differ substantially from those found with B8 in solution. Moreover, the effect of the nature of the core substituent on the CS and CR dynamics in the octachromophoric systems has been investigated by comparing the new red octachromophoric molecule R8 with B8 in solution. The photophysics of R8 and B8 have also been compared with those of the red and blue single NDI units, R1 and B1, respectively, and with that of a blue bichromophoric system (B2).

Experimental Section

Samples. The synthesis of R1 and R8 has been described in ref 38 and that of B1, B2, and B8 in ref 36. The solvents acetonitrile (ACN) and methanol (MeOH) were used without further purification. Tetracyanoethylene (TCNE) was recrystallized and sublimed, whereas *N*,*N*-dimethylaniline (DMA) and nitrobenzene (NB) were distilled before use. For steady-state and time-correlated single photon counting experiments, the concentration in terms of NDI units was on the order of 10 μM. For fluorescence up-conversion and TA experiments, they amounted to about 1 mM and to 300 μM, respectively. LUVs were prepared as described in ref 36. Namely, a solution of egg yolk phosphatidylcholine (10 mg) in $CHCl_3$/MeOH 1:1 was dried using a rotary evaporator and then under vacuum (>2 h). The resulting dried lipid was hydrated for >30 min (1 mL, 10 mM potassium phosphate, 100 mM KCl, pH 7.0), freeze−thawed (5×), extruded through a polycarbonate membrane (15×, pore size 100 nm), and diluted with the buffer (4 mL, 10 mM potassium phosphate, 100 mM KCl, pH 7.0) to give LUVs dispersion. Incorporation of B8 in LUVs was accomplished by the addition of the MeOH solution of B8 to the gently stirred LUVs dispersion.

Steady-State Measurements. Absorption spectra were recorded on a Cary 50 spectrophotometer, whereas fluorescence and excitation spectra were measured on a Cary Eclipse fluorimeter. All fluorescence spectra were corrected for the wavelength-dependent sensitivity of the detection. Quantum yield measurements were performed against cresyl violet (Φ_{fl} = 0.53)[39] or rhodamine 6 G (Φ_{fl} = 0.94) in ethanol.[40]

Time-Resolved Measurements. Excited-state lifetime measurements on the nanosecond time scale were carried out with the time-correlated single photon counting technique as described earlier.[14] Excitation was performed at a repetition rate of 10 MHz with ~60 ps pulses generated with laser diodes at 395 and 469 nm (Picoquant models LDH-P-C-400B and LDH-P-C-470). The full width at half-maximum of the instrument response function was around 200 ps and the accuracy on the lifetimes of ca. 0.1 ns.

Lifetime measurements on shorter time scales were performed using fluorescence up-conversion. The experimental setup has been described in detail elsewhere.[41] Excitation was achieved at 400 nm with the frequency-doubled output of a Kerr lens mode-locked Ti:Sapphire laser (Tsunami, Spectra-Physics). The output pulses centered at 800 nm had 100 fs duration and 82 MHz repetition rate. The polarization of the pump beam was at magic angle relative to that of the gate pulses at 800 nm. The 400 nm pump intensity on the sample was on the order of 5 $\mu J \cdot cm^{-2}$. The sample solutions were located in a 1 mm rotating cell. The full width at half-maximum of the instrument response function was ca. 280 fs.

The experimental setup for TA measurements has been described in detail earlier.[42] Excitation was performed either at 530 or at 620 nm with a home-built two-stage noncollinear optical parametric amplifier,[43] fed by the 800 nm output of a standard 1 kHz amplified Ti:Sapphire system (Spectra-Physics). The pump intensity at the sample was around 2 $mJ \cdot cm^{-2}$. The polarization of the probe pulses was at magic angle relative to that of the pump pulses. After acquisition, all spectra were corrected for the chirp of the white light probe pulses. The full width at half-maximum of the instrument response function was

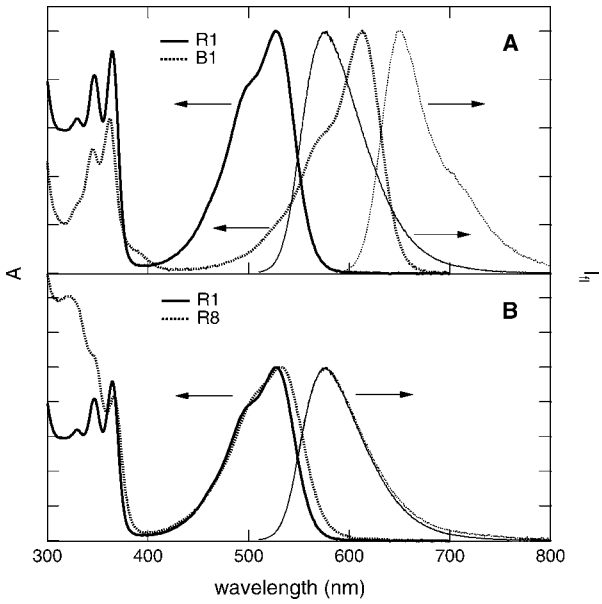

Figure 2. Absorption (thick line) and fluorescence (thin line) spectra of R1, R8, and B1 in MeOH.

ca. 200 fs. The sample solutions were kept in a 1 mm thick quartz cell and were continuously stirred by N_2 bubbling. Their absorbance at the excitation wavelength was about 0.3.

Quantum Chemistry Calculations. Ground-state gas-phase geometry optimization was performed at the density functional level of theory (DFT) using the BP86 functional[44] and a [3s2p1d] basis set.[45] The calculations were carried out using Turbomole version 5.9.[46,47]

Results

Steady-State Spectra. The absorption spectra of the red and blue NDI units, R1 and B1, in MeOH (Figure 2A) are essentially identical to those already reported for the same chromophores but with different substituents on the imide nitrogens.[34] The intense absorption band in the visible region originates from a charge-transfer transition associated with the naphthalene-core substituents, whereas the band with a maximum around 365 nm comes from a $\pi\pi^*$ transition involving only the NDI center and is independent of core substitution. These features are mostly preserved in the bi- and octachromophoric systems as illustrated in Figure 2B with R1 and R8. In these systems, the electronic transition that corresponds to the S_0-S_1 transition in a single NDI unit will be called S_0-LES (locally excited state) transition. As will be shown later on, electronic excited states with lower energy and delocalized over several NDI units or involving both an NDI unit and the *p*-octiphenyl scaffold are also present.

The S_0-LES band of R8 is slightly broader on its red side than that of R1 and red-shifted by about 150 cm^{-1}. On the other hand, absorption arising from the *p*-octiphenyl scaffold of R8 can be observed below 400 nm, additionally to that of the NDI $\pi\pi^*$ transition. The spectral changes observed by going from B1 to B8 differ somewhat, as the S_0-LES band of B8 is broader on both sides than that of B1 but peaks at the same wavelength, this effect being already present with B2. Finally, this band broadens further in the LUV membrane and a shoulder at 598 nm can be noticed, as already discussed in ref 36. The presence of this shoulder, assigned to an excitonic transition, together with a strong circular dichroism signal in this spectral region were considered as evidence of the self-organization of the B8s into the $B8_4$ tetramer in the LUV membrane.[36,48]

TABLE 1: Fluorescence Quantum Yields, Φ_{fl}, and Average Lifetimes, $\langle\tau_{fl}\rangle$

	environment	Φ_{fl}	$\langle\tau_{fl}\rangle$ (ns)
R1	MeOH	0.08	2.3
R1	ACN	0.51	9.4[a]
R8	MeOH	0.01	0.21
B1	MeOH	0.32	8.4
B2	MeOH	0.05	2.1
B8	MeOH	0.01	0.20
$B8_4$	LUV	~0.001	0.12

[a] Fluorescence up-conversion measurements were not performed.

The fluorescence spectra of R1 and R8 in MeOH are essentially undistinguishable. Interestingly, the fluorescence excitation spectra of R1 and R8 are also identical and are very similar to the absorption spectrum of R1. This indicates that the broadening of the S_0-LES absorption band of R8 is most probably associated with the presence of a nonfluorescent subpopulation. The same behavior is found with the blue systems, both fluorescence and excitation spectra of B1, B2, and B8 being alike. The S_0-LES band observed in the fluorescence excitation spectra of B2 and B8 is also narrower than in the corresponding absorption spectra.

Surprisingly, the fluorescence quantum yields, Φ_{fl}, of R1 and B1 differ greatly (Table 1). The low Φ_{fl} value of R1 in the protic MeOH can be attributed to the occurrence of H-bond assisted nonradiative deactivation of the excited state,[49–51] which probably involves intermolecular proton transfer.[52,53] Indeed, the fluorescence quantum yield of R1 in nonprotic solvents like ACN and DMSO is 4−6 times larger. This deactivation pathway of the excited state is apparently not operative with B1. One possible reason is the presence of strong intramolecular H-bonds between the two amino substituents and the nearest carbonyl oxygen atoms, which prevents intermolecular proton transfer. Such protecting effect is no longer possible with the chlorine substituent.

Independently of this, the fluorescence quantum yields of the multichromophoric systems are much smaller than those of R1 and B1. A further reduction of Φ_{fl} is observed with B8 in the LUV membrane. However, because of their size (100 nm diameter), the LUVs strongly scatter excitation light, making the detection of weak fluorescence problematic. As a consequence, the relative error on Φ_{fl} in LUVs is considerable ($\pm$100%).

Time-Resolved Fluorescence Measurements. The early fluorescence dynamics of all five molecules in MeOH and of B8 in the LUV membrane recorded at the maximum wavelength is displayed in Figure 3. The time profile measured with B1 is the simplest and can be reproduced using a biexponential function with a 1 ps rising component and an 8.4 ns decaying component. The rise time was found to shorten by going to B2 and B8 in MeOH. On the other hand, the fluorescence rise of B8 in the LUV membrane and of R1 and R8 is prompt. The rising component can in principle originate from vibrational or solvent relaxation. Solvent relaxation is unlikely, as it should yield the same rise time for all compounds. Moreover rather different time constants than those found here have been reported for the solvation dynamics in MeOH.[54] Vibrational relaxation seems more plausible as excitation is performed at 400 nm, i.e., with about 1.1 eV more energy than the S_0-S_1 0−0 transition. The shorter rise time observed by going from B1 to B8 might be associated with the increasing size of the molecule, which favors rapid intramolecular redistribution of the vibrational energy.[55]

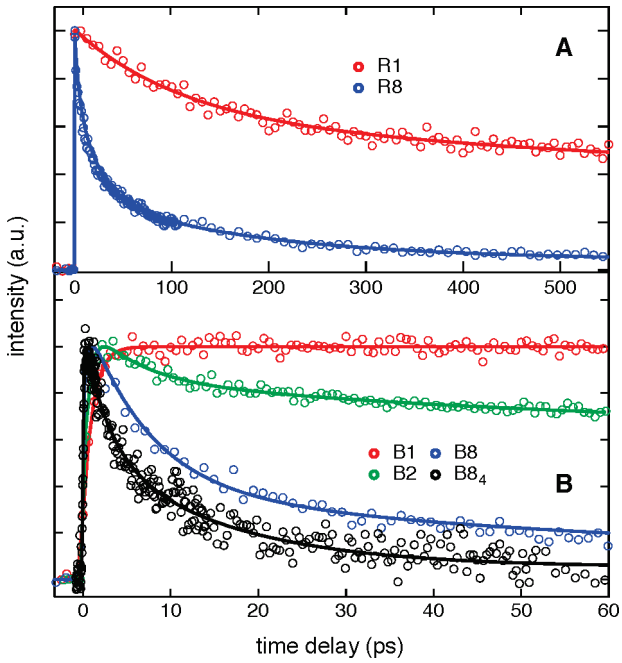

Figure 3. Time profiles of the fluorescence intensity of the red (A) and blue (B) systems recorded at the band maximum upon 400 nm excitation and best multiexponential fits (solid line).

TABLE 2: Time Constants and Relative Amplitudes (in Parentheses) Obtained from Analysis of the Fluorescence Time Profiles at the Peak Wavelength

	τ_1 (ps)	τ_2 (ps)	τ_3 (ps)	τ_4 (ps)	τ_5 (ns)	τ_6 (ns)
R1				115 (0.39)	1.6 (0.32)	6.0 (0.29)
R8		4.3 (0.24)	23 (0.44)	164 (0.26)	1.4 (0.03)	4.3 (0.02)
B1	1.0 (−0.72)					8.4 (1.0)
B2	0.70 (−1.0)	5.7 (0.24)	63 (0.20)	980 (0.24)	4.0 (0.20)	8.4 (0.12)
B8	0.55 (−1.0)	7.1 (0.66)	51 (0.19)	160 (0.12)	1.8 (0.01)	7.3 (0.02)
B8$_4$		2.8 (0.45)	15 (0.50)	770 (0.03)		5.0 (0.02)

Although less excess excitation energy (∼0.8 eV) has to be dissipated in the red systems, a similar effect could have been anticipated. A possible reason for the prompt rise of fluorescence might be the existence of intermolecular H-bonds, which are known to enhance vibrational energy relaxation.[56]

Structural relaxation of the molecules in the excited state, which often follows electronic transitions with some charge-transfer character as is the case here, could also be responsible for this early fluorescence dynamics. It should be noted that these fluorescence time profiles have been recorded at a single wavelength. An unambiguous assignment of the origin of this dynamic feature (vibrational relaxation, solvation, and/or structural relaxation) would require measurement of the early fluorescence dynamics at wavelengths covering the whole emission band.

The fluorescence decays of all compounds but B1 are strongly nonexponential and require at least three exponential functions to be satisfactorily reproduced. The corresponding lifetimes and associated amplitudes are listed in Table 2, while the average lifetimes are listed in Table 1. These tables show that the small fluorescence quantum yield measured with R1 in MeOH arises from a shorter excited-state lifetime because of the existence of a H-bond assisted nonradiative deactivation pathway, involving most probably intermolecular proton transfer, that is not operative in ACN. The different decay components observed with R1 in MeOH could be accounted for by a different excited-state proton-transfer efficiency of the regioisomers.

Despite this, it appears clearly that the reduced fluorescence quantum yield of the multichromophoric systems originates, at least partially, from an additional nonradiative deactivation pathway that is nonexistent in R1 and B1. This point will be discussed in more detail below.

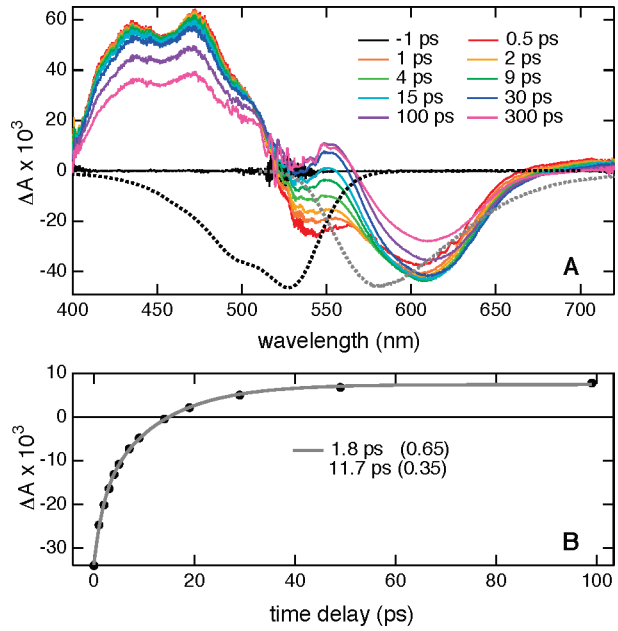

Figure 4. (A) TA spectra measured with R1 in MeOH at various time delays after 530 nm excitation (solid line) together with the negative steady-state absorption and stimulated emission spectra (dotted line). (B) Temporal evolution of the TA signal intensity at 545 nm and best biexponential fit (solid line).

TA Measurements. ***Red Systems.*** TA spectra recorded with R1 in MeOH upon 530 nm excitation are shown in Figure 4A. The main features are a broad positive band between 400 and 510 nm and a broad negative band centered around 620 nm. As the amplitude of the positive TA band exhibits a time evolution similar to that found by time-resolved fluorescence, this band can be assigned to S_1-state absorption. Similarly, the negative signal above 550 nm can be ascribed to S_1-S_0 stimulated emission. However, this negative band is 30 nm red-shifted relative to the stimulated emission spectrum of R1, calculated by multiplying its steady-state fluorescence intensity by λ^4.[57] Moreover, no negative signal due to the bleach of the S_0-S_1 absorption can be observed around 530 nm. This indicates that the S_1-state absorption spectrum of R1 most probably extends over the whole visible region and masks the ground-state bleach signal and the blue side of the stimulated emission spectrum.

In the 530−560 nm region, the signal intensity is negative at short time delays and positive after about 20 ps (Figure 4B). This change is accompanied by a red shift of the stimulated emission band on the same time scale. The early TA dynamics at 545 nm can be reproduced with a biexponential function with time constants of 2 and 12 ps, and relative amplitudes of 0.65 and 0.35, respectively. These values are close to the 2.5 and 15 ps time constants reported for the solvation dynamics of coumarin 153 in MeOH.[54] As a consequence, these early spectral changes in the 530−560 nm region can be assigned to dynamic Stokes shift of the stimulated emission. This effect was not observed in the time-resolved fluorescence measurements because they were performed at the band maximum where the Stokes shift does not result in a very significant intensity variation. As discussed above, vibrational and structural relaxation of the excited state could also be partially involved in this early dynamics. Once relaxation is complete, the TA

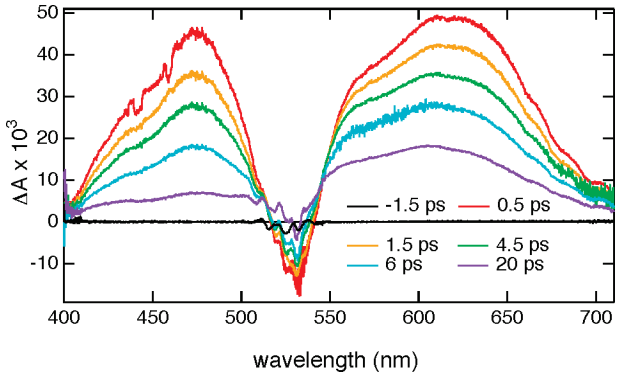

Figure 5. TA spectra recorded with R1 + 4 M DMA in MeOH at various time delays after 530 nm excitation.

intensity in this region is positive because of the predominance of S_1-state absorption. This spectral dynamics together with the strong spectral overlap make an extraction of the intrinsic S_1-state absorption spectrum hardly possible.

In order to identify the spectra of R1 radical ions, TA measurements with solutions of R1 in MeOH in the presence of either an electron donor or an electron acceptor have been performed. The transient spectra shown in Figure 5 and obtained with R1 and 4 M DMA in MeOH differ substantially from those in pure MeOH: the negative band around 620 nm is replaced by a positive band culminating at about the same wavelength and the secondary maximum at 435 nm is missing. The absence of stimulated emission can easily be explained by the quenching of R1 in the S_1 state upon electron transfer from DMA. This very rapid quenching can be accounted for by the high quencher concentration, 4 M DMA in MeOH corresponding to a 1:1 (v/v) DMA/MeOH mixture, as subpicosecond time constants have been reported for the quenching of several excited chromophores in pure DMA.[58–60] As a consequence, the transient spectra should be dominated by the absorption of the quenching product, namely, the radical anion $R1^{\bullet -}$ and the radical cation $DMA^{\bullet +}$, as well as by the bleach of the S_0-S_1 absorption. As $DMA^{\bullet +}$ is known to only exhibit a weak absorption band around 475 nm,[61] all the positive TA features come from $R1^{\bullet -}$, whereas the negative signal at 532 nm originates from the bleach of the ground-state absorption. Core-unsubstituted NDI anions have an intense absorption band peaking around 475 nm,[26,28,32] in good agreement with the TA band at 473 nm found here. The other TA band above 550 nm might arise from an additional transition of $R1^{\bullet -}$ involving the core substituents. The signal intensity throughout the whole TA spectrum exhibits a biphasic decay with time constants of 4 ps and >100 ps with relative amplitudes 0.9 and 0.1, respectively, that arises from geminate CR of the $DMA^{\bullet +}/R1^{\bullet -}$ pairs. The biphasic nature of the decay could come from the presence of ion pairs with different coupling, namely, tight and loose ion pairs.[62] However, this hypothesis was not further investigated, this going beyond the scope of the present study. Trials to identify the absorption spectrum of $R1^{\bullet +}$ by using the electron acceptor TCNE as quencher were unsuccessful. Indeed no other transient bands than those observed with R1 alone could be detected. This could be explained either by an $R1^{\bullet +}$ absorption spectrum located outside the spectral window of the experiment or by an ion population that is too small to give a significant signal intensity as CR of the ion pair is much faster than quenching.

The transient spectra measured with R8 in MeOH (Figure 6A) differ substantially from those recorded with R1. The 400−500 nm region of R8 resembles somewhat that of R1

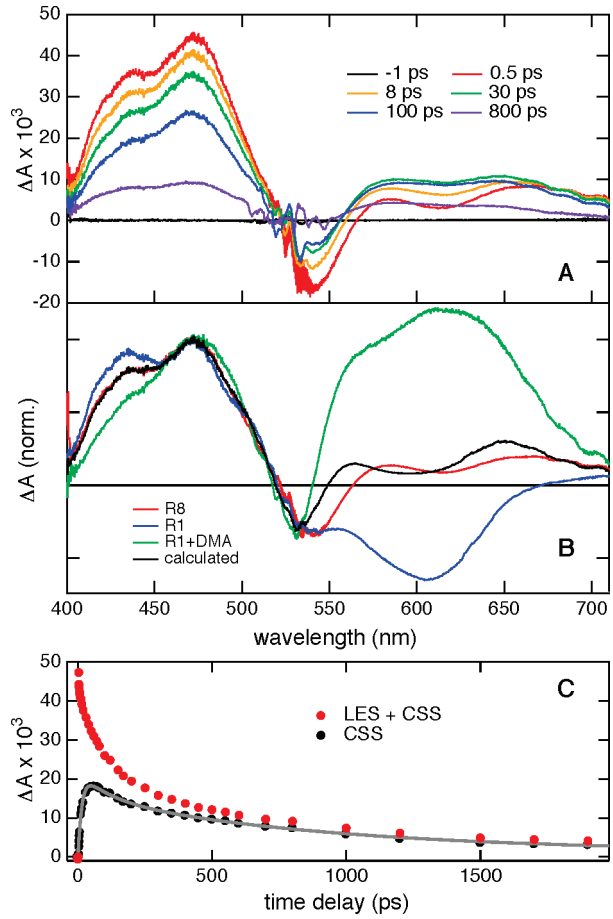

Figure 6. (A) TA spectra recorded with R8 in MeOH at various time delays after 530 nm excitation. (B) TA spectrum measured with R8, 5 ps after excitation (red), and TA spectrum calculated (black) by a linear combination of spectra measured with R1 alone (blue) and with DMA (green) at the same time delay. (C) Time evolution of the TA intensity at 470 nm before (red) and after (black) subtraction of the contribution of the LES population and best fit of eq 1 (gray).

except that the secondary maximum at 435 nm is now only a shoulder. On the other hand, the negative TA signal caused by stimulated emission is replaced by a broad positive band of medium intensity. During the first 30 ps, some spectral evolution can be observed above 550 nm: the shallow 620 nm minimum present at early time has almost completely vanished after 30 ps. This change originates from a decrease of the stimulated emission concomitant with an increase of a positive TA signal. The interpretation of these TA spectra is greatly facilitated by the time-resolved fluorescence data, which show that the decay of the LES population is triphasic (Table 2), and that, although most of this population has decayed after 100 ps, a residual LES population is still present up to several nanoseconds. As a consequence, the transient spectra of R8 at all time delays contain contributions from the unquenched LES and from another population resulting from the quenched LES population. As illustrated in Figure 6B, the TA spectrum of R8 below 530 nm can be perfectly well reproduced by a linear combination of the transient spectra recorded at the same time delay with R1 alone and with DMA. The agreement on the red side of the spectrum is not as good but is qualitatively reasonable, considering that the dynamic Stokes shift of the stimulated fluorescence might differ for R1 and R8 because of different environments of the chromophores. Thus, the TA spectra of R8 point to the presence of both an LES and a charge-separated state (CSS) population. In the latter state, the negative charge is clearly on

a red NDI chromophore. However, the location of the hole cannot be inferred from the TA spectra. This point is discussed in the next section.

Figure 6C shows the time profile of the TA intensity at 470 nm reflecting both LES and CSS population dynamics. In order to estimate the temporal evolution of the CSS population only, the contribution of the LES population was removed by subtracting the time profile measured by fluorescence. The scaling factor was taken from the weight of the TA spectrum of R1 alone used to reproduce the spectrum of R8 in Figure 6B. The resulting profile, also shown in Figure 6C, now reflects the temporal evolution of the CSS population but does in principle not allow the intrinsic lifetime of this population to be extracted. This would indeed only be possible if the CSS were populated instantaneously, which is clearly not the case here.

The observed time dependence of the TA signal due the CSS population, $A_{CSS}^{obs}(t)$, can be mathematically expressed by the following convolution integral:[62]

$$A_{CSS}^{obs}(t) = c\int_0^t P_{CSS}^{int}(t-t')F(t)\,dt \quad (1)$$

where c is a constant, $P_{CSS}^{int}(t)$ is the time profile of CSS population that would be observed if this state were populated instantaneously, and $F(t)$ is its time-dependent buildup rate. The latter can be deduced from the decay of the LES population upon CS, $P_{LES}^{CS}(t)$:

$$F(t) = -\frac{\partial P_{LES}^{CS}(t)}{\partial t} \quad (2)$$

$P_{LES}^{CS}(t)$ can be obtained from the ratio of the fluorescence time profiles of R8 and R1:

$$P_{LES}^{CS}(t) = \frac{I_{R8}(t)}{I_{R1}(t)} \quad (3)$$

In the latter equation, the acceleration of the fluorescence decay by going from R1 to R8 is assumed to stem from CS only. Table 2 shows that $P_{LES}^{CS}(t)$ can be reasonably well described by a biexponential function with time constants of 4.3 and 23 ps and relative amplitudes of 0.35 and 0.65, respectively.

The continuous line in Figure 6C is the best fit of eq 1 to the temporal evolution of the CSS population using for $P_{CSS}^{int}(t)$ a biexponential function with time constants of 98 ps and 1.1 ns and relative amplitudes of 0.35 and 0.65, respectively. These two largely different time constants do not automatically imply two distinct CSS subpopulations but most probably reflect a distribution of subpopulations with different relative orientations of the chromophores and thus CR time constants ranging from less than 100 ps to more than 1 ns.

Blue Systems. The TA spectra of B1 in MeOH upon 620 nm excitation (Figure 7A) share some similarity with those of R1, with a broad positive band between 400 and 590 nm with maxima at about 510 and 570 nm and a broad negative band centered around 625 nm. The first feature can be safely assigned to the S_1 state of B1, whereas the negative band arises from both stimulated S_1-S_0 emission and bleach of the S_0-S_1 absorption. However, the S_0-S_1 absorption band extends to much shorter wavelengths than the negative TA band and overlaps strongly with the S_1-state absorption spectrum. Some spectral dynamics, such as an increase of the relative intensity of the 510 and 570 nm maxima and a red shift of the negative TA band, can be observed during the first 30 ps. As a consequence, the early time evolution of the TA signal intensity

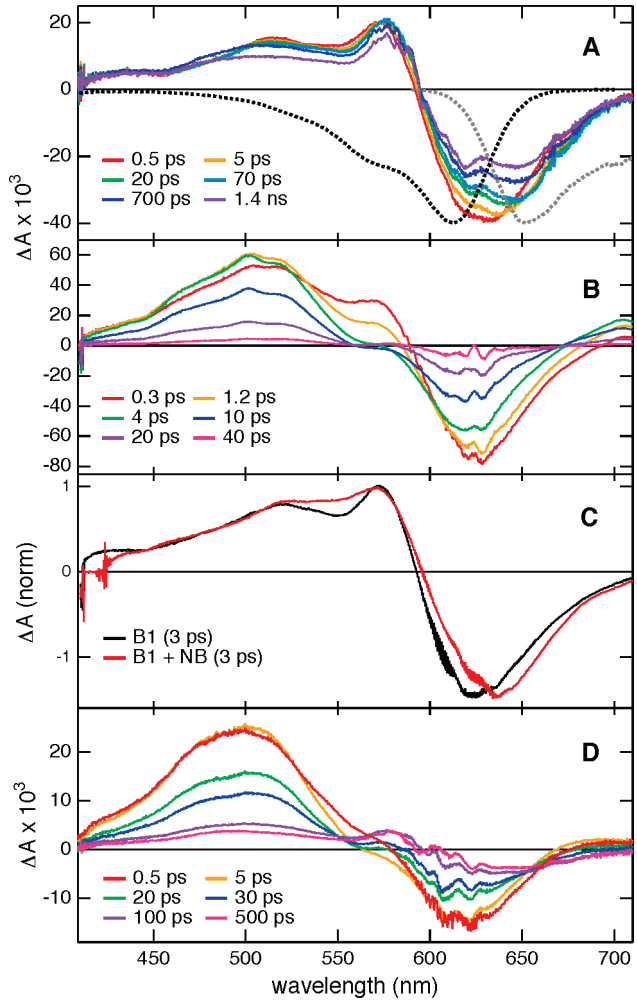

Figure 7. TA spectra measured with B1 in MeOH (A), B1 in MeOH + 3 M DMA (B), B1 in MeOH and in NB (C), and B2 in MeOH (D), at various time delays after 620 nm excitation. (The dotted spectra in (A) are the negative steady-state absorption and stimulated emission spectra of B1.)

at almost any wavelength can be reproduced by a biexponential function with 2 and 16 ps time constants. These values are very close to those found with R1 in MeOH and can be similarly assigned to solvent relaxation, with some possible contribution from vibrational and structural relaxation. After this process, the TA signal intensity remains almost constant over the time window of the experiment (0−2 ns) in agreement with the 8.4 ns fluorescence lifetime of B1.

The TA spectra of B1 with 3 M DMA differ substantially from those in pure MeOH (Figure 7B). At short time delays, the presence of B1 in the S_1 state can still be recognized by the stimulated emission in the red part of the negative TA band and as the small positive shoulder at 570 nm. As time proceeds, the contribution of the S_1-state population decreases to zero as testified by the blue shift of the negative TA band due to the quenching of the stimulated fluorescence and by the disappearance of the 570 nm shoulder. After about 3 ps, the TA spectrum consists of a broad positive band centered at 502 nm, of a negative band due only to the bleach of the S_0-S_1 absorption, and of a positive feature above 680 nm. All the positive TA bands can be assigned to the radical anion $B1^{\bullet-}$. The decay of the intensity of both the $B1^{\bullet-}$ and bleach bands can be reproduced with a biexponential function with time constants of 9.7 and 38 ps and relative amplitudes of 0.89 and 0.11, respectively. These time constants differ substantially from those

found with R1 and DMA, probably because of different driving forces for both CS and CR. It should be noted that the TA spectra recorded with B1 are not largely different from those measured with R1, the main dissimilarities being essentially caused by the location of the bands associated with the S_0-S_1 bleach and the stimulated emission.

As for R1, attempts to observe the radical cation $B1^{\bullet+}$ generated upon quenching by the strong electron acceptor TCNE failed. The measurements were repeated with B1 in pure NB, which has the advantage over TCNE to be a substantially weaker electron acceptor (E_{red}(NB) = −1.15 V vs SCE,[63] E_{red}(TCNE) = +0.24 V vs SCE).[64] Therefore, CR of the resulting ion pair should be more exergonic and thus slower, as predicted for electron-transfer processes in the inverted regime.[65] As illustrated in Figure 7C, the transient spectrum of B1 in NB is almost the same as that in MeOH except for a larger relative intensity in the 550 nm region and a red shift of the negative band. Interaction between R1 in the S_1 state and NB is supported by the strong reduction of the excited-state lifetime compared to MeOH. Indeed, the decay of the stimulated emission at 650 nm can be reproduced by a biexponential function with time constants of 43 and 215 ps and relative amplitudes of 0.27 and 0.73, respectively, clearly much smaller than the 8.4 ns lifetime in MeOH. However, the shape of the TA spectrum does not change significantly with time. The most plausible explanation is that the interaction of B1 in the S_1 state and NB does not result to a true geminate ion pair with full charge transfer but rather to an exciplex with only a partial charge-transfer character. This is a well-known effect when the driving force for CS is unfavorable as is the case here with $\Delta G_{CS} \sim 0.3$ eV.[66,67] Therefore, the transient spectra of B1 in NB can be assigned to the S_1 state of B1 perturbed by a charge-transfer interaction with NB. The absorption spectrum of $B1^{\bullet+}$ can unfortunately not be deduced from these data.

The early TA spectra measured with B2 in MeOH (Figure 7D) are very similar to those found with B1 + DMA (Figure 7B), pointing to the occurrence of CS. However, as time proceeds, the TA features associated with the CSS decay and a residual spectrum very similar to that recorded with B1 alone (Figure 7A) is observed. The small shoulder around 570 nm can be seen at all time delays, and the maximum of the negative TA band remains red-shifted relative to that measured with DMA, indicating the continuous presence of an LES population. This agrees with the time-resolved fluorescence measurements that show that about 12% of the LES population decay with an 8.4 ns time constant. Thus, the CSS population decays before that of the LES, explaining the TA spectrum at long time delay. The simultaneous presence of LES and CSS populations complicates the determination of the CR time constant. The time profile of the TA signal intensity at 500 nm exhibits a prompt rise and a slower rise with an ~4 ps time constant followed by a biphasic decay with 22 ps and >1 ns time constants. The prompt rise can be assigned to the initial LES population, and the slower one to the buildup of the CSS population. Its time constant is consistent with the 5.7 ps found in the fluorescence decay of B2. The 22 ps decay time reflects the disappearance of the CSS population, whereas the >1 ns component is due to the residual LES population. If one considers eqs 2 and 3 and Table 2, it appears that $F(t)$ can be reasonably well reproduced by a biexponential function with time constants of 5.7 and 63 ps and relative amplitudes of 0.93 and 0.07, respectively. From this and from eq 1, it is evident that a substantial CSS population is generated within a few picoseconds, and therefore, the 22 ps

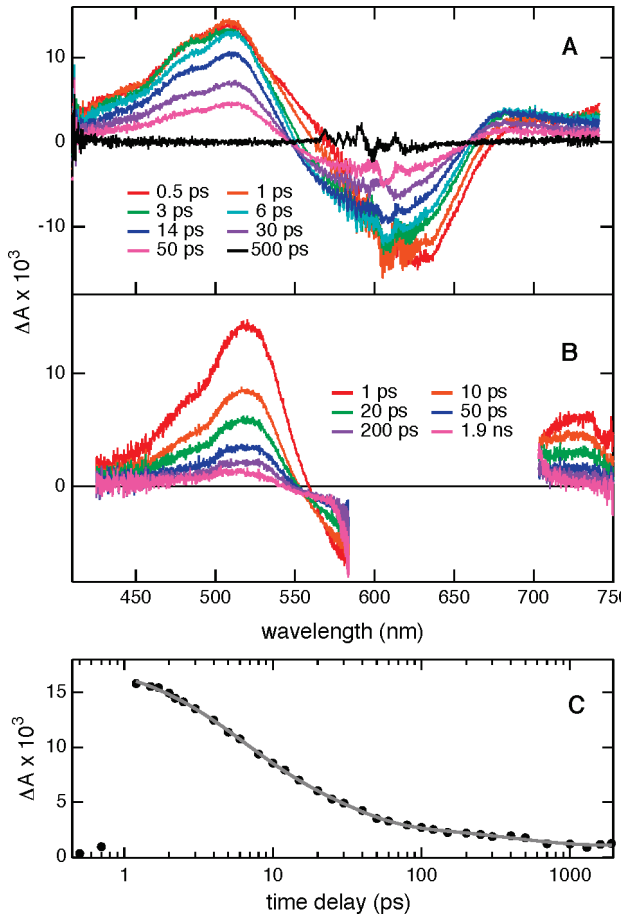

Figure 8. TA spectra recorded with B8 in MeOH (A), and $B8_4$ in the LUV membrane (B), at various time delays after 620 nm excitation. (C) Temporal evolution of the TA signal intensity at 515 nm measured with $B8_4$ in the LUV membrane and best multiexponential fit (gray line).

decay component of the TA intensity at 570 nm gives a good estimate of the intrinsic CR time constant.

The TA spectra of B8 in MeOH (Figure 8A) are very similar to those measured with B1 and DMA and are thus dominated by CSS absorption and the bleach of the S_0-LES absorption. The contribution of the LES can be guessed at early time as a shoulder around 570 nm. The temporal evolution of the signal intensity at essentially any wavelength can be reproduced by a biexponential function with 2−4 and 40−45 ps time constants. Depending on the wavelength, the associated amplitudes are of the same or opposite sign. The shortest time constant is most probably related to solvation (and possibly vibrational relaxation) and to the decay of the LES population upon CS. On the other hand the 40−45 ps can be assigned to CR, as it leads to the decay of the CSS population and to the ground-state recovery. Although the spectra associated with both LES and CSS overlap, the time scales of buildup and decay of the CSS population differ sufficiently to allow the assignment of the 40−45 ps time constant to the intrinsic CR time constant without using eq 1.

The TA spectra of $B8_4$ measured in the LUV membrane are shown in Figure 8B. The spectral region between 600 and 700 nm is totally hidden by the scattering of the excitation light by the LUVs. Nevertheless, the spectra in the remaining regions are dominated by CSS absorption and no contribution from the LES can be detected. The time dependence of the CSS population differs substantially from that found in MeOH as illustrated in Figure 8C. The time profile of the TA intensity in

TABLE 3: Energetic Parameters for CS and CR in the Multichromophoric Systems[a]

donor/acceptor	ΔG_{CS} (eV)	ΔG_{CR} (eV)
R/R	−0.08	−2.25
S/R	+0.01	−2.34
B/B	−0.05	−1.95
S/B	+0.43	

[a] Calculated with $E_{LES}(R) = 2.33$ eV; $E_{red}(R) = -0.72$ V; $E_{ox}(R) = 1.53$ V; $E_{LES}(B) = 2.0$ eV; $E_{red}(B) = -0.81$ V; $E_{ox}(B) = 1.14$ V; $E_{ox}(S) \approx E_{ox}(QA) = 1.62$ V (all potentials are vs SCE and taken from ref 38).

the 515 nm region cannot be reproduced with less than the sum of three exponential functions with time constants of 5, 25, and 400 ps and relative amplitudes of 0.49, 0.40, and 0.11, respectively. A possible origin of such multiphasic CR dynamics is discussed in the next section.

Discussion

Nature of the Charge-Separated State. The reduction of fluorescence quantum yield and fluorescence lifetime observed by going from the single NDI units to the multichromophoric systems evidence the existence of an additional decay pathway of the LES in the latter systems. Furthermore, the presence of TA bands that can be assigned to the NDI anion unambiguously points to the occurrence of CS. No TA band that could be ascribed to the radical cation could be detected in the spectra. To our knowledge, the absorption spectrum of an NDI radical cation has never been reported so far. The TA spectra indicate that, if generated, the NDI radical cations should not absorb significantly in the spectral window of the experiment or should have an absorption spectrum similar to that of the anion. On the other hand, the scaffold of R8 and B8 is equivalent to an octianisole that could potentially act as electron donor. The absorption spectrum of octianisole radical cation should not differ much from that of anisole radical cation, which is known to exhibit a weak band around 450 nm.[61] As the TA spectra of R8 and B8 are dominated in this region by the relatively intense bands of both the LES and the radical anion, the presence of the hole on the scaffold can neither be confirmed nor rejected. On the other hand, the feasibility of CS between an excited NDI chromophore and the scaffold can be estimated by considering its driving force:[68]

$$\Delta G_{CS} = -E_{LES} - E_{red}(A) + E_{ox}(D) \qquad (4)$$

where E_{LES} is the energy of the LES, and $E_{red}(A)$ and $E_{ox}(D)$ are the reduction and oxidation potentials of the electron acceptor and donor, respectively. The correction factor, C, that accounts for the electrostatic interaction between the resulting ionic moieties has been omitted here as it is generally accepted to be very small in polar solvents, $C \approx -0.05$ eV. The ΔG_{CS} values for CS between two chromophores (R/R or B/B) and between the scaffold and an excited chromophore (S/R or S/B) are listed in Table 3. It is immediately clear that CS between two chromophoric units is energetically feasible in both red and blue systems but that CS to the scaffold should only be operative in R8 (Figure 9). This trend has been confirmed by recent fluorescence quenching measurements of R1 and B1 in ACN by quateranisole (QA) and hexamethylbenzene (HMB), which have similar oxidation potentials ($E_{ox}(QA) = 1.62$ V vs SCE, and $E_{ox}(HMB) = 1.59$ V vs SCE).[38] The fluorescence of R1 is efficiently quenched by HMB with a rate constant of 4×10^9 M^{-1} s^{-1}. Moreover, a reduction of the fluorescence lifetime of R1 from 9.4 to 5.2 ns was observed upon addition of 29 mM

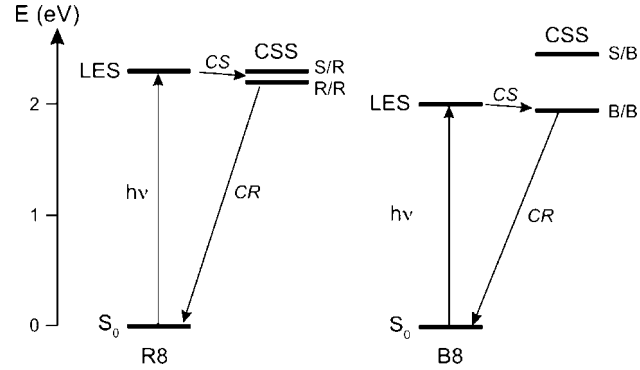

Figure 9. Energy level scheme accounting for CS and CR in the octachromophoric systems (the energies of the CSS should be considered as upper limits as the electrostatic interaction has been neglected).

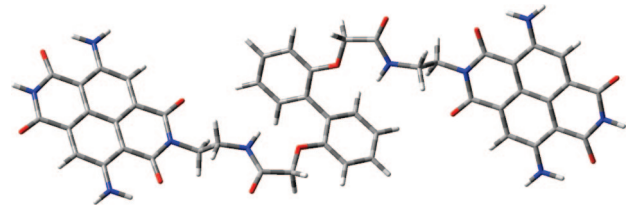

Figure 10. Gas-phase equilibrium geometry of a B2 analogue.

QA, corresponding to a quenching rate constant similar to that with HMB. On the other hand, the fluorescence intensity of B1 was unaffected by the presence of HMB, in agreement with a largely positive ΔG_{CS}.

In summary, the hole in B2 and B8 is most certainly located on an NDI chromophore. With R8 on the other hand, both CS pathways might be operative (Figure 9). A hopping of the hole from a chromophore to the scaffold and vice versa should also be feasible. Symmetry-breaking CS in perylene mono- and diimide dimers,[19,20] as well as in π-stacked perylenediimides,[20,21] has also been reported by Wasielewski and co-workers. In these systems, CS was found to primarily occur between strongly coupled chromophores with cofacial π-stacked geometry. Indication of CS in dimers with an edge-to-edge arrangement of the chromophores was found in polar solvents only.

Charge-Separation Dynamics. Figure 10 shows the gas-phase equilibrium geometry of a B2 analogue calculated at the DFT level of theory. In order to accelerate the calculations, all N-substituents have been replaced by H-atoms. In this geometry, the through-space edge-to-edge distance between the chromophores amounts to 14.5 Å. This distance is clearly much too large to account for the ultrafast decay components of B2 fluorescence and the presence of the anion band in the TA spectra already at short time delays. Considering the relatively weak driving force for CS, this distance would rather be compatible with the nanosecond components of the fluorescence decay. Through-bond CS can also be reasonably excluded as the through-bond edge-to-edge distance is as large as 24.7 Å. It is, however, clear that the bridges linking the chromophores to the scaffold are flexible and that B2 can adopt many other geometries at room temperature. Moreover, torsional disorder of the *p*-oligophenyl scaffold[69,70] further increases the number of possible conformations of B2 and of the octachromophoric systems. The mutual orientation of the chromophores is thus obviously not unique. Furthermore, the observation that the S_0−LES absorption band of the multichromophoric systems differs from that of the single NDI units, whereas the fluorescence excitation spectra are identical, points to the existence of

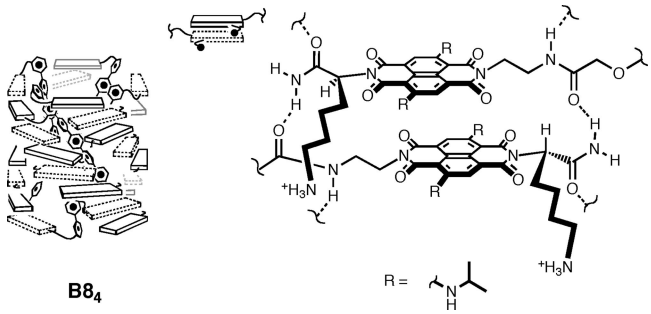

Figure 11. Schematic structure of the tetramer $B8_4$.

a nonemitting subpopulation. This subpopulation may be associated with geometries where two chromophores are sufficiently coupled to lead to a delocalization of the electronic excitation and thus to excitonic splitting.[71] As a consequence, the absorption spectrum may shift or broaden according to the mutual orientation of the chromophores. The radiative rate constant also strongly depends on this relative orientation and totally vanishes in a H-dimer where the chromophores have a cofacial arrangement. However in the present case, even if the relative geometry of the chromophores is not that of a nonemitting H-dimer, the fluorescence is prevented by ultrafast CS. The geometries where the chromophores are far apart and that where they form a dimer most probably correspond to the extreme limits of a broad distribution of mutual orientations. This distribution is at the origin of the nonexponential fluorescence decay of R8, B2, and B8 (see Table 2) and thus of a distribution of CS time scales going from a few picoseconds to a few nanoseconds.

In the case of R8, the coupling between an NDI unit and the scaffold is most certainly smaller than that between two cofacial chromophores. Therefore, the ultrafast fluorescence decay components in R8 most probably originate from CS between two chromophores and not from CS with the scaffold.

In the LUV membrane, four B8s have been shown to self-organize by π-stacking into a quadruple M-helices architecture, $B8_4$, where four chromophores of a B8 unit interdigitate with four chromophores of an adjacent B8 unit (Figure 11).[36,48] This self-organization results to a small interchromophoric distance, hence to large coupling. Indeed, the 32 chromophores in the $B8_4$ assembly are ordered as four π-stacks that could be viewed as four H-type aggregates. Excitonic interaction in such an arrangement is responsible for the substantial broadening of the blue side of the S_0-LES absorption band of $B8_4$ in the LUV membrane, whereas the helicity of the π-stacks accounts for the circular dichroism signal.[48] The radiative rate constant of such H-aggregates can be expected to be substantially smaller than that of the individual chromophores. This agrees well with the 10-fold reduction of the fluorescence quantum yield of $B8_4$ in the LUV membrane compared to B8 in MeOH, whereas the average fluorescence lifetime is reduced by less than a factor 2. Thus, ultrafast CS upon excitation of such aggregated dyes is equivalent to exciton dissociation. Molecular dynamics simulations of the $B8_4$ reveal that the mutual geometry of the chromophores is not unique,[36] although the distribution is much narrower than in MeOH. As a consequence, a distribution of CS rate constants should also be expected. The data in Table 2 show that 90% of the fluorescence decays with a 15 ps or shorter time constant, the residual fluorescence vanishing much more slowly. The latter is most probably caused by B8 molecules that are present as monomers or by defective supramolecular assemblies.

TABLE 4: Time Constants and Relative Amplitudes (in Parentheses) for CR in the Multichromophoric Systems Obtained from Analysis of the TA Data

	$\tau_{CR,1}$ (ps)	$\tau_{CR,2}$ (ps)	$\tau_{CR,3}$ (ps)	$\langle\tau_{CR}\rangle$ (ps)
R8	98 (0.35)	1100 (0.65)		750
B2	22 (1)			22
B8	45 (1)			45
$B8_4$	5 (0.49)	25 (0.40)	400 (0.11)	56

CR Dynamics. The CR time constants determined from TA data analysis are summarized in Table 4. The CR dynamics does not only depend on the chromophores but also on their number and their relative position as shown by the differences between B2 and B8 in MeOH and in the LUV membrane. It should first be noted that the single CR time constants found with B2 and B8 in MeOH do not imply that there is a unique CR time scale in these two systems. Indeed, a substantial CS state population can only be observed if CR is slower than CS (see eq 1). In the case of B2, it is thus not possible to resolve CR components shorter than about 5 ps. Similarly, the CSS population generated in the slowest phase of CS, associated with 63 and 980 ps time constants, does not contribute to the TA signal unless it recombines with longer time constants. Therefore, the 22 ps time constant measured with B2 can be attributed to the recombination of the CSS population generated with the 5 ps time constant. However a CR component of this population shorter than 5 ps cannot be excluded. This 22 ps time constant is reasonable considering that it corresponds to the recombination of relatively well-coupled ions. Time constants of the same order of magnitude have been observed in geminate ion pairs with similar driving force for CR.[72] In polar solvents, this driving force corresponds to the onset of the inverted regime as predicted by the semiclassical theory of nonadiabatic electron-transfer reactions.[65]

Although the fastest CS components found in B2 and B8 are similar, CR in the latter is twice as slow. A major difference between these two systems is that, apart from recombining, the charges in B8 can hop to a nearby neutral chromophore. Such charge migration should considerably lengthen the lifetime of the CSS population. This process does not alter CSS population, and its occurrence cannot be seen in the TA spectra. However, unless the chromophores are perfectly parallel to each other, electron hopping should lead to a depolarization of the radical anion band. Polarized TA measurements, that will be described in detail elsewhere, indeed reveal a much faster decay of the polarization with B8 in MeOH than with B2. The same effect is probably responsible for the slow CR component found with $B8_4$ in the LUV membrane. In this case, the charges can migrate over 32 chromophores arranged in four parallel π-stacks. As the coupling between the chromophores within a stack is considerable, both charge hopping and recombination should be very fast. This certainly explains the 5 and 25 ps CR components. On the other hand, the edge-to-edge distance between chromophores in two adjacent stacks is of the order of 4−5 Å. Therefore, although the coupling between such dyes is relatively small, some lateral migration of the charges should also be operative. As the survival time of two opposite charges in different stacks is definitely larger than for two charges in the same stack, such lateral hopping is most probably at the origin of the 400 ps CR component.

The decay of the CSS population in R8 is much slower than in B8, the ratio of the average CR time constants being as large as 16. According to Table 3, the driving force for CR, $\Delta G_{CR} = -E_{LE} - \Delta G_{CS}$, is larger by 0.3 eV in R8 than in B8 (Figure 9).

Thus, according to nonadiabatic electron-transfer theory, CR in R8 should be more in the inverted regime. Such an increase of ΔG_{CR} in this driving force range was found to change from 22 to 170 ps the CR time constant of geminate ion pairs produced upon bimolecular fluorescence quenching of cyanoanthracenes by DMA in ACN.[72] As a consequence, the 1.1 ns CR time constant in R8 is difficult to account for only in terms of an increased driving force. As discussed above, both CS with a second chromophore and with the scaffold have a quite similar driving force. Therefore, the hole can in principle hop to both another chromophore and the scaffold while the electron is confined in the chromophores. This difference in charge localization should greatly enhance the CSS lifetime, as it should strongly decrease the probability of encounter of holes and electrons. As CS with the scaffold is energetically not possible with B8, these distinct paths for hole and electron hopping do not exist with this system, and thus the charges have a much higher recombination probability.

Excitation Energy Hopping and Exciton Annihilation. As shown in Figure 2, the absorption and fluorescence spectra of both red and blue chromophores overlap substantially, and therefore, the occurrence of excitation energy hopping (EEH) in the multichromophoric systems should be considered. The Förster radius for EEH via the Coulombic interaction has been estimated to 57 and 42 Å for red and blue chromophores, respectively, assuming random orientation of the energy donors and acceptors. On the other hand, the calculated center-to-center distance between the chromophores in B2 is at most 22 Å. Therefore, optical excitation of the multichromophoric systems should be followed by both CS and EEH. This is confirmed by steady-state measurements of the fluorescence of B1, B2, and B8 in low-temperature MeOH glasses that reveal that the fluorescence of B1 is polarized, whereas that of B2 and B8 is not. This depolarization of the emission is a direct consequence of EEH between two randomly oriented chromophores. Time-resolved fluorescence anisotropy measurements are being currently performed in order to determine the EEH dynamics.

Finally, exciton annihilation is known to be a major deactivation pathway of excited states in aggregates and multichromophoric systems.[4,73–75] This process manifests by a dependence of the fluorescence quantum yield and of the excited-state dynamics on the excitation intensity. Exciton annihilation can be viewed as an energy transfer from an excited chromophore to another excited chromophore yielding the donor in the electronic ground state and the acceptor in a highly excited state. Additionally to the excitation intensity, its efficiency depends on the overlap of the fluorescence and excited-state absorption spectra as in "conventional" Förster-type energy transfer. As significant overlap of LES and stimulated emission spectra can be seen in the TA spectra of R1 and B1 (Figures 4A and 7A), exciton annihilation could in principle take place in the multichromophoric systems, especially in R8, B8, and $B8_4$, the probability to have more than one excitation per molecule increasing with the number of chromophores. At the pump intensity of 2 $mJ \cdot cm^{-2}$ used in the TA experiments, the average number of excitations/chromophore can be estimated to amount to $p = 0.08$. The probability, P_x, to have x excitations/system is given by the binomial distribution:[76,77]

$$P_x = \frac{n!}{x!\,(n-x)!} p^x (1-p)^{n-x} \qquad (5)$$

where n is the number of chromophores/system. For R8 and B8, these probabilities are: $P_1 = 0.36$, $P_2 = 0.11$, $P_3 = 0.02$, and $P_{n>3} \approx 0$. As the lifetime of an excitation in R8, B8, and $B8_4$ is very small, exciton annihilation should not play a significant role in the excited-state dynamics reported here. However, because this process is too slow to compete with CS, the excitation of more than one chromophore in a system results in the generation of several electron/hole pairs. This in turn should lead to an acceleration of CR in its initial phase and to a recombination dynamics that depends on the excitation intensity. This effect has not been investigated but could partially account for the ultrafast CR component observed with $B8_4$. However, the slower part of the recombination dynamics should not be influenced by multiple excitations.

Concluding Remarks

The results described here illustrate the remarkable properties of core-substituted NDI-based multichromophoric systems. Most multichromophoric structures investigated so far exhibit only excitation energy hopping upon optical excitation. On the contrary, those studied here are essentially nonfluorescent because of very efficient CS. This process occurs on a wide range of time scales, going from a few picoseconds to a few nanoseconds, despite a modest driving force. The key parameter controlling CS in these systems is not the driving force but the electronic coupling, which is influenced by both distance and mutual orientation of the participating groups. CR dynamics is similarly influenced by the electronic coupling but is additionally complicated by the possibility for the charges to hop to a nearby neutral chromophore. Therefore, CR depends also strongly on the number of chromophoric units. The dynamics of this charge migration is being currently investigated by polarization-sensitive TA. Finally, the difference between the absorption and fluorescence excitation spectra found mainly with B2 and B8 indicates that the strongly coupled and thus nonfluorescent chromophores absorb preferentially on the edges of the S_0-LES absorption band. Consequently, both CS and CR dynamics should exhibit a substantial dependence on the excitation wavelength. Experimental confirmation of such a spectral effect is planned in our laboratory.

In conclusion, the photophysical properties of these multichromophoric systems make them highly interesting building blocks for the design of sophisticated photoactive systems as recently demonstrated.[36,38,78]

Acknowledgment. This work was supported by the Fonds National Suisse de la Recherche Scientifique through Project Nos. 200020-115942 and 200020-117593.

References and Notes

(1) Berberan-Santos, M. N.; Canceill, J.; Gratton, E.; Jullien, L.; Lehn, J.-M.; So, P.; Sutin, J.; Valeur, B. *J. Phys. Chem.* **1996**, *100*, 15.

(2) Kuclauskas, D.; Liddell, P. A.; Lin, S.; Johnson, T. E.; Weghorn, S. J.; Lindsey, J. S.; Moore, A. L.; Moore, T. A.; Gust, D. *J. Am. Chem. Soc.* **1999**, *121*, 8604.

(3) Yeow, E. K. L.; Ghiggino, K. P.; Reek, J. N. H.; Crossley, M. J.; Bosman, A. W.; Schenning, A. P. H. J.; Meijer, E. W. *J. Phys. Chem. B* **2000**, *104*, 2596.

(4) Morandeira, A.; Vauthey, E.; Schuwey, A.; Gossauer, A. *J. Phys. Chem. A* **2004**, *108*, 5741.

(5) Hwang, I.-W.; Ko, D. M.; Ahn, T. K.; Yoon, Z. S.; Kim, D.; Peng, X.; Aratani, N.; Osuka, A. *J. Phys. Chem. B* **2005**, *109*, 8643.

(6) Sautter, A.; Kaletas, B. K.; Schmid, D. G.; Dobrawa, R.; Zimine, M.; Jung, G.; Van Stokkum, I. H. M.; De Cola, L.; Williams, R. M.; Wuerthner, F. *J. Am. Chem. Soc.* **2005**, *127*, 6719.

(7) Oesterling, I.; Muellen, K. *J. Am. Chem. Soc.* **2007**, *129*, 4595.

(8) Garcia-Parajo, M. F.; Hernando, J.; Mosteiro, G. S.; Hoogenboom, J. P.; van Dijk, E. M. H. P.; van Hulst, N. F. *ChemPhysChem* **2005**, *6*, 819.

(9) Grozema, F. C.; Houarner-Rassin, C.; Prins, P.; Siebbeles, L. D. A.; Anderson, H. L. *J. Am. Chem. Soc.* **2007**, *129*, 13370.

(10) Masuo, S.; Vosch, T.; Cotlet, M.; Tinnefeld, P.; Habuchi, S.; Bell, T. D. M.; Oesterling, I.; Beljonne, D.; Champagne, B.; Muellen, K.; Sauer, M.; Hofkens, J.; De Schryver, F. C. *J. Phys. Chem. B* **2004**, *108*, 16686.
(11) de Silva, A. P.; McClenaghan, N. D. *Chem.—Eur. J.* **2004**, *10*, 574.
(12) Yang, S.; Tian, H. *Trends Photochem. Photobiol.* **2002**, *9*, 55.
(13) Rye, H. S.; Yue, S.; Wemmer, D. E.; Quesada, M. A.; Haugland, R. P.; Mathies, R. A.; Glazer, A. N. *Nucleic Acids Res.* **1992**, *20*, 2803.
(14) Fürstenberg, A.; Julliard, M. D.; Deligeorgiev, T. G.; Gadjev, N. I.; Vassilev, A. A.; Vauthey, E. *J. Am. Chem. Soc.* **2006**, *128*, 7661.
(15) Terenziani, F.; Mongin, O.; Katan, C.; Bhattula, B. K. G.; Blanchard-Desce, M. *Chem.—Eur. J.* **2006**, *12*, 3089.
(16) Sundström, V.; Pullerits, T.; van Grondelle, R. *J. Phys. Chem. B* **1999**, *103*, 2327.
(17) Vauthey, E.; Suppan, P.; Haselbach, E.; Davidson, R. S. *Helv. Chim. Acta* **1986**, *69*, 430.
(18) Kovalenko, S. A.; Lustres, J. L. P.; Ernsting, N. P.; Rettig, W. *J. Phys. Chem.* **2003**, *107*, 10228.
(19) Fuller, M. J.; Gusev, A. V.; Wasielewski, M. R. *Isr. J. Chem.* **2004**, *44*, 101.
(20) Fuller, M. J.; Sinks, L. E.; Rybtchinksi, B.; Giaimo, J. M.; Li, X.; Wasielewski, M. R. *J. Phys. Chem. A* **2005**, *109*, 970.
(21) Rybtchinski, B.; Sinks, L. E.; Wasielewski, M. R. *J. Am. Chem. Soc.* **2004**, *126*, 12268.
(22) Green, S.; Fox, M. A. *J. Phys. Chem.* **1995**, *99*, 14752.
(23) Barros, T. C.; Brochsztain, S.; Toscano, V. G.; Berci Filho, P.; Politi, M. J. *J. Photochem. Photobiol., A* **1997**, *111*, 97.
(24) Alp, S.; Erten, S.; Karapire, C.; Koz, B.; Doroshenko, A. O.; Icli, S. *J. Photochem. Photobiol., A* **2000**, *135*, 103.
(25) Abraham, B.; McMasters, S.; Mullan, M. A.; Kelly, L. A. *J. Am. Chem. Soc.* **2004**, *126*, 4293.
(26) Andric, G.; Boas, J. F.; Bond, A. M.; Fallon, G. D.; Ghiggino, K. P.; Hogan, C. F.; Hutchison, J. A.; Lee, M. A. P.; Langford, S. J.; Pilbrow, J. R.; Troup, G. J.; Woodward, C. P. *Aust. J. Chem.* **2004**, *57*, 1011.
(27) Refat, M. S.; Grabchev, I.; Chovelon, J. M.; Ivanova, G. *Spectrochim. Acta, Part A* **2006**, *64A*, 435.
(28) Ganesan, P.; Baggerman, J.; Zhang, H.; Sudholter, E. J. R.; Zuilhof, H. *J. Phys. Chem. A* **2007**, *111*, 6151.
(29) Greenfield, S. R.; Svec, W. A.; Gosztola, D.; Wasielewski, M. R. *J. Am. Chem. Soc.* **1996**, *118*, 6767.
(30) Hayes, R. T.; Wasielewski, M. R.; Gosztola, D. *J. Am. Chem. Soc.* **2000**, *122*, 5563.
(31) Guo, X.; Gan, Z.; Luo, H.; Araki, Y.; Zhang, D.; Zhu, D.; Ito, O. *J. Phys. Chem. A* **2003**, *107*, 9747.
(32) Borgstroem, M.; Shaikh, N.; Johansson, O.; Anderlund, M. F.; Styring, S.; Aakermark, B.; Magnuson, A.; Hammarstroem, L. *J. Am. Chem. Soc.* **2005**, *127*, 17504.
(33) Ghiggino, K. P.; Hutchison, J. A.; Langford, S. J.; Latter, M. J.; Lee, M. A. P.; Takezaki, M. *Aust. J. Chem.* **2006**, *59*, 179.
(34) Würthner, F.; Shahadat, A.; Thalacker, C.; Debaerdemaeker, T. *Chem.—Eur. J.* **2002**, *8*, 4742.
(35) Thalacker, C.; Roeger, C.; Wuerthner, F. *J. Org. Chem.* **2006**, *71*, 8098.
(36) Bhosale, S.; Sisson, A. L.; Talukdar, P.; Fürstenberg, A.; Banerji, N.; Vauthey, E.; Bollot, G.; Mareda, J.; Röger, C.; Würthner, F.; Sakai, N.; Matile, S. *Science* **2006**, *313*, 84.
(37) Sakai, N.; Sisson, A. L.; Bhosale, S.; Fürstenberg, A.; Banerji, N.; Vauthey, E.; Matile, S. *Org. Biomol. Chem.* **2007**, *5*, 2560.
(38) Sisson, A. L.; Sakai, N.; Banerji, N.; Fürstenberg, A.; Vauthey, E.; Matile, S. *Angew. Chem., Int. Ed.* **2008,***47,*3727.
(39) Madge, D.; Brannon, J. H.; Cremers, T. L.; Olmsted, J., III *J. Phys. Chem.* **1979**, *83*, 695.
(40) Fischer, M.; Georges, J. *Chem. Phys. Lett.* **1996**, *260*, 115.
(41) Morandeira, A.; Engeli, L.; Vauthey, E. *J. Phys. Chem. A* **2002**, *106*, 4833.
(42) Duvanel, G.; Banerji, N.; Vauthey, E. *J. Phys. Chem. A* **2007**, *111*, 5361.
(43) Wilhelm, T.; Piel, J.; Riedle, E. *Opt. Lett.* **1997**, *22*, 1494.
(44) Perdew, J. P. *Phys. Rev. B* **1986**, *33*, 8822.
(45) Schäfer, A.; Horn, H.; Ahlrichs, R. *J. Chem. Phys.* **1992**, *97*, 2571.
(46) Ahlrichs, R.; Bär, M.; Häser, M. *Chem. Phys. Lett.* **1989**, *162*, 165.
(47) Häser, M.; Ahlrichs, R. *J. Comput. Chem.* **1989**, *10*, 104.
(48) Bhosale, S.; Matile, S. *Chirality* **2006**, *18*, 849.
(49) Flom, S. R.; Barbara, P. F. *J. Phys. Chem.* **1985**, *89*, 4489.
(50) Shimada, H.; Nakamura, A.; Yoshihara, T.; Tobita, S. *Photochem. Photobiol. Sci.* **2005**, *4*, 367.
(51) Mohammed, O. F.; Vauthey, E. *J. Phys. Chem. A* **2008,***112,*3823.
(52) Agmon, N. *J. Phys. Chem. A* **2005**, *109*, 13.
(53) Fürstenberg, A.; Vauthey, E. *Photochem. Photobiol. Sci.* **2005**, 260.
(54) Horng, M. L.; Gardecki, J. A.; Papazyan, A.; Maroncelli, M. *J. Phys. Chem.* **1995**, *99*, 17311.
(55) Nesbitt, D. J.; Field, R. W. *J. Phys. Chem.* **1996**, *100*, 12735.
(56) Pigliucci, A.; Duvanel, G.; Lawson Daku, M. L.; Vauthey, E. *J. Phys. Chem. A* **2007**, *111*, 6135.
(57) Perez-Lustres, J. L.; Rodriguez-Prieto, F.; Mosquera, M.; Senyushkina, T. A.; Ernsting, N. P.; Kovalenko, S. A. *J. Am. Chem. Soc.* **2007**, *129*, 5408.
(58) Kandori, H.; Kemnitz, K.; Yoshihara, K. *J. Phys. Chem.* **1992**, *96*, 8042.
(59) Engleitner, S.; Seel, M.; Zinth, W. *J. Phys. Chem. A* **1999**, *103*, 3013.
(60) Morandeira, A.; Fürstenberg, A.; Gumy, J.-C.; Vauthey, E. *J. Phys. Chem. A* **2003**, *107*, 5375.
(61) Shida, T. *Electronic Absorption Spectra of Radical Ions*; Elsevier: Amsterdam, 1988; Vol. Physical Sciences Data *34*.
(62) Pagès, S.; Lang, B.; Vauthey, E. *J. Phys. Chem. A* **2004**, *108*, 549.
(63) Jensen, B. S.; Parker, V. D. *J. Chem. Soc, Chem. Commun.* **1974**, *10*, 367.
(64) Ganesan, V.; Rosokha, S. V.; Kochi, J. K. *J. Am. Chem. Soc.* **2003**, *125*, 2559.
(65) Marcus, R. A.; Sutin, N. *Biochim. Biophys. Acta* **1985**, *811*, 265.
(66) Kikuchi, K.; Niwa, T.; Takahashi, Y.; Ikeda, H.; Miyashi, T.; Hoshi, M. *Chem. Phys. Lett.* **1990**, *173*, 421.
(67) Kuzmin, M. G. *J. Photochem. Photobiol., A* **1996**, *102*, 51.
(68) Rehm, D.; Weller, A. *Isr. J. Chem.* **1970**, *8*, 259.
(69) Almenningen, A.; Bastiansen, O.; Fernholt, L.; Cyvin, B. N.; Cyvin, S. J.; Samdal, S. *J. Mol. Struct.* **1985**, *128*, 59.
(70) Poater, J.; Sola, M.; Bickelhaupt, F. M. *Chem.—Eur. J.* **2006**, *12*, 2889.
(71) Kasha, M.; Rawls, H. R.; El-Bayoumi, M. A. *Pure Appl. Chem.* **1965**, *11*, 371.
(72) Vauthey, E. *J. Phys. Chem. A* **2001**, *105*, 340.
(73) Sundström, V.; Gillbro, T.; Gadonas, R. A.; Piskarskas, A. *J. Chem. Phys.* **1988**, *89*, 2754.
(74) Gadonas, R.; Feller, K.-H.; Pugzlys, A.; Jonusauskas, G.; Oberlé, J.; Rullière, C. *J. Chem. Phys.* **1997**, *106*.
(75) van Amerongen, H.; Valkunas, L.; van Grondelle, R. *Photosynthetic Excitons*; World Scientific: Singapore, 2000.
(76) Paillotin, G.; Swenberg, C. E.; Breton, J.; Geacintov, N. E. *Biophys. J.* **1979**, *25*, 513.
(77) Parson, W. W. *Modern Optical Spectroscopy*; Springer: Berlin, 2007.
(78) Sakai, N.; Sisson, A. L.; Bürgi, T.; Matile, S. *J. Am. Chem. Soc.* **2007**, *129*, 15758.

JP801276P